## Title

Depth-of-interaction study of a dual-readout detector based on TOFPET2 application-specific integrated circuit.



## Journal

Physics in Medicine & Biology, 64(17)

## Authors

Li, Mohan
Abbaszadeh, Shiva

## Publication Date

2019-09-04

## DOI

10.1088/1361-6560/ab3866

Peer reviewed

HHS Public Access

Author manuscript

*Phys Med Biol*. Author manuscript; available in PMC 2020 May 20.

Published in final edited form as:

*Phys Med Biol*. ; 64(17): 175008. doi:10.1088/1361-6560/ab3866.

# Depth-of-interaction study of a dual-readout detector based on TOFPET2 application-specific integrated circuit

**Mohan Li**, **Shiva Abbaszadeh**

Department of Nuclear, Plasma, and Radiological Engineering, University of Illinois at Urbana-Champaign, Urbana, IL 61801, United States of America

## Abstract

Depth-of-interaction (DOI) capability is important for achieving high spatial resolution and sensitivity in dedicated organ and small animal positron emission tomography (PET) scanners. The dual-ended readout is one of the common methods that can achieve good DOI resolution. The aim of this study is to evaluate a dual-ended readout detector based on silicon photomultiplier (SiPM) and TOFPET2 application-specific integrated circuit (ASIC). The detector is based on 4 × 4 lutetium–yttrium oxyorthosilicate (LYSO) units, each unit contained 6 × 6 LYSO crystals, and the crystal size was 1 × 1 × 20 $mm^3$. The four lateral surfaces of LYSO crystals were mechanically ground to W14 (surface roughness 10–14 $\mu$m), and the two ended surfaces were polished (surface roughness,<0.5 $\mu$m). The reflector was Toray Lumirror E60, and the packing fraction of the LYSO block was 86.5%. Each LYSO unit was read out from both ends with two Hamamatsu S13361-3050AE-08 SiPM arrays. The analog output signals of SiPM were digitized by PETsys TOFPET2 ASIC and acquired by PETsys SiPM Readout System. The ASIC and SiPM were cooled by a fan and a Peltier element. To investigate the crystal resolvability, different light guide thicknesses including 0.8, 1, 1.2 and 2 mm were tested. The light guide was made of optical glass (H-K9L-Foctek Photoincs), and the size and refractive index were 6.45 × 6.45 $mm^2$ and 1.53 (at 420 nm), respectively. To characterize the detector performance at different depths, another 1 × 25.8 × 20 $mm^3$ single LYSO slab was used. Data were acquired at 10 depths (1, 3, …, 19 mm), and each depth had a 10 min acquisition time and about 40 thousand coincidence events. During the experiment, the SiPM temperature was controlled as 27.6 ± 0.4 °C. The results showed that the 1.2 mm light guide offered the best crystal resolvability. The energy, coincidence time, and DOI resolution full-width at half-maximum of the detector were characterized as 15.66% ± 0.66%, 602.98 ± 10.58 ps, and 2.33 ± 0.07 mm, respectively. The good DOI resolution indicates the potential of utilizing the detector for high-resolution PET applications.

### Keywords

dual-ended readout; PET; depth-of-interaction; TOFPET2 ASIC

mohanli2@illinois.edu.

## 1. Introduction

In high-resolution positron emission tomography (PET) applications such as dedicated organ (brain or breast) imaging and small animal imaging, spatial resolution and photon coincidence sensitivity are two of the most important properties (Burr *et al* 2004, Yang *et al* 2016). While spatial resolution determines the capability of resolving neighboring lesions, sensitivity determines the signal-to-noise ratio of the reconstructed image. To achieve high sensitivity, long crystals are utilized, and compact geometry is preferred so that a large solid angle of field of view (FOV) can be covered. However, systems with long crystals and compact geometry suffer from parallax error, which degrades the spatial resolution (Dokhale *et al* 2004, St James *et al* 2009). In cylindrical scanners, for example, the radial spatial resolution component degrades gradually with the increase of the radial offset from the scanner center, and axial resolution is also degraded in the 3D acquisition. Fortunately, parallax error can be mitigated by using detectors with depth-of-interaction (DOI) capability (Stickel and Cherry 2004, Yang *et al* 2008).

Different DOI detector configurations including, but not limited to, dual-ended readout, single-ended readout, side readout, and monolithic scintillator detector have been investigated for PET applications, as follows:

- Dual-ended readout uses two detectors that are coupled to both ends of crystals and DOI is estimated as the ratio of signal amplitudes of the two detectors (Moses and Derenzo 1994). In such a configuration, DOI is continuous, uniform and the resolution full-width at half-maximum (FWHM) can be smaller than 2 mm in 20 mm lutetium–yttrium oxyorthosilicate (LYSO) (Kuang *et al* 2017). However, dual-ended readout doubles the number of detectors and readout channels, which increases the cost.
- Single-ended readout needs auxiliary techniques. For example, pulse shape discrimination is used to extract DOI from different layers of the crystal bar, which have different timing properties (Berg *et al* 2016). Another example is sharing light between neighboring crystals so that DOI is encoded by considering the extent of light dispersion (Ito *et al* 2010). DOI can also be decoded by using a light guide as the reflector on the other end of the crystal array (Pizzichemi *et al* 2016). The DOI resolution of single-ended readout is about 2–5 mm for 20 mm LSYO.
- Side readout reads signals from crystal lateral surfaces instead of end surfaces. In such a configuration, the DOI resolution equals to the scintillator crystal crystal size, which is 5–7 mm (Yamaya *et al* 2006, Yeom *et al* 2014). Higher DOI resolution can be achieved by reducing the crystal length, but more scintillator layers will be needed to maintain high sensitivity. Since the lateral surface area is larger than the ended surface area, the cost of side readout is higher than dual-ended and single-ended readout. The detectors within crystal layers also lower the packing fraction.
- A monolithic scintillator detector encodes DOI by calibration. Though it reduces the inter-crystal dead space and DOI resolution smaller than 2 mm can be

achieved in 10 mm LYSO (Schaart *et al* 2009), the spatial resolution at the edges of the crystal is degraded, and the calibration of monolithic-scintillator-based detectors requires complicated procedures.

Among all depth encoding approaches, dual-ended readout has the advantage to achieve the highest DOI resolution and spatial resolution with a better light-collection efficiency (Godinez *et al* 2012). In recent years, silicon photomultiplier (SiPM) has been investigated for dual-ended readout detectors (Du *et al* 2018, Kuang *et al* 2018). Compared with PMT and APD, SiPM has advantages such as compact size, high gain, low bias voltage, good timing property, and low sensitivity to magnet field (Bisogni and Morrocchi 2016). The compact size is especially important for a dual-ended readout configuration because photosensors on one end of the scintillator have to face FOV and thus a compact photosensor can effectively reduce the scanner geometry.

TOFPET2 is an application-specific integrated circuit (ASIC) for time and amplitude measurements of SiPM signals (Di Francesco *et al* 2016, Bugalho *et al* 2018). Though TOFPET2 ASIC is specifically designed for time-of-flight applications, the low-noise and low-power features make it suitable for dual-ended readout, where the number of channels is larger. The aim of this study is to evaluate a dual-ended readout detector based on SiPM and TOFPET2 ASIC. The detector performances characterized as crystal resolvability, coincidence time resolution, energy resolution, and DOI resolution are reported.

## 2. Materials and methods

### 2.1. Scintillator and photosensor

The scintillator was chosen as LYSO due to its fast and high light output (Kimble *et al* 2002). The LYSO block (Epic Crystal, China) was based on 4 × 4 units. Each LYSO unit contained 6 × 6 LYSO crystals, and the crystal size was 1 × 1 × 20 $mm^3$. The four lateral surfaces of LYSO crystals were ground to W14 (roughness 10–14 $\mu$m) and the two ended surfaces were polished (roughness <0.5 $\mu$m). The reflector was Toray Lumirror E60 (Toray Industries Inc., Japan), with thickness of 0.05 mm. With optical glue, the crystal array pitch size was 1.06 mm. As a result, the LYSO unit size was 6.45 × 6.45 $mm^2$, the LYSO block size was 25.8 × 25.8 $mm^2$. For one LYSO unit, the effective crystal size was 6 × 6 $mm^2$, and the entire size was 6.45 × 6.45 $mm^2$, so the packing fraction was computed as 86.5%. For the entire LYSO block, the effective crystal size was 24 × 24 $mm^2$, and the entire size was 25.8 × 25.8 $mm^2$, so the packing fraction was still 86.5%.

To extract the DOI information, two Hamamatsu S13361-3050AE-08 SiPM arrays (Hamamatsu Photonics, Japan) were coupled to both ends of the LYSO block with BC-630 optical grease (Saint-Gobain Crystals, US). One SiPM array contained 8 × 8 SiPM channels and each channel had a 3 × 3 $mm^2$ effective photosensitive area. The SiPM array size was 25.8 mm, which was the same as the LYSO block. In this experiment, different SiPM channels were triggered and read out independently. Different LYSO unit had its own light guide, i.e. a 4 × 4 light guide array. As a result, each LYSO unit was read out by two 2 × 2 SiPM arrays, as shown in figure 1.

### 2.2. Crystal resolvability

Because the LYSO crystal size (1 × 1 $mm^2$) was smaller than the SiPM channel size (3 × 3 $mm^2$), two H-K9L optical light guides (Foctek Photonics Inc., Japan) were coupled to both ends of each LYSO unit to share the scintillation light to multiple SiPM channels for resolving crystal (Yamamoto *et al* 2016). The previous study shows that the crystal identification capability is affected by the light guide thickness (Song *et al* 2010). Briefly, with a thin light guide, the light sharing among SiPMs is inefficient and LYSO crystals in the corner of the SiPM array are difficult to distinguish. When the light guide is thick, however, the excessive light sharing will result in a reduced crystal separation because neighboring crystals have similar light sharing patterns. To investigate the optimal light guide thickness, four LYSO units with different thicknesses included 0.8, 1, 1.2 and 2 mm were fabricated, as shown in figure 2.

The experiment setup for measuring the optimal light guide thickness is shown in figure 3. The analog output signals of SiPMs were digitized by PETsys TOFPET2 ASIC (PETsys Electronics SA, Portugal) and acquired by PETsys SiPM Readout System. Whenever a SiPM channel got triggered, a timing output and an energy output would be read out and recorded. The SiPM operating voltage was set as 56 V and the discriminator values ($vth_t1$ = 20, $vth_t2$ = 20, $vth_e$ = 15) were chosen based on the PETsys user manual. Using these parameters, the threshold value was about 5–6 photoelectrons. The ASIC and SiPM were cooled by a fan and a Peltier element. A 30-$\mu$Ci Na-22 source (Eckert & Ziegler Inc., Germany) was used to irradiate the LYSO unit from side. Each LYSO unit had a 10 min data acquisition time. During the experiment, the SiPM temperature was controlled as 29.2 ± 0.3 °C.

The $x$ and $y$ coordinates of the flood histogram were calculated using the position-encoding energy signals from the two 2 × 2 SiPM arrays as Ren *et al* (2014)

$$x = \frac{1}{2}\left(\frac{B_1 + C_1}{E_1} + \frac{B_2 + C_2}{E_2}\right),\ y = \frac{1}{2}\left(\frac{C_1 + D_1}{E_1} + \frac{C_2 + D_2}{E_2}\right), \quad (1)$$

where $A_1$, $B_1$, $C_1$ and $D_1$ are the four energy outputs from the SiPM array on the one end of the LYSO unit and $A_2$, $B_2$, $C_2$ and $D_2$ are from the SiPM array on the other end. $E_1$ and $E_2$ are the total energy measured by the two SiPM arrays respectively as

$$E_1 = A_1 + B_1 + C_1 + D_1,\ E_2 = A_2 + B_2 + C_2 + D_2\,. \quad (2)$$

Since different SiPM channels were read out independently, only events that could trigger all 4 SiPM channels on either end of the LYSO unit were selected.

### 2.3. Energy, time and DOI resolution

After optimizing the light guide thickness, the LYSO block was fabricated and placed into the two SiPM arrays. To characterize the energy, time and DOI resolutions of the designed detector at different depths, another single 1 × 25.8 × 20 $mm^3$ LYSO slab was used. The LYSO slab was also read out by a Hamamatsu S13361-3050AE-08 SiPM array with 8 SiPM channels. As shown in figure 4, the LYSO slab and the Na-22 source were placed on a

translation stage, which could move along the depth direction of the LYSO block. The source active diameter was 0.25 mm. The distance from the LYSO block to the source was 20 mm, and the distance from the LYSO slab to the source was also 20 mm. Since the width of the slab was 1 mm, the incident beam width in this experiment was 1 mm. Data were acquired at 10 depths (1, 3, …, 19 mm), and each depth had a 10 min acquisition time. Two-$\sigma$ energy window was used for each LYSO unit at different depth, and each depth had about 40 thousand coincidence events. During the experiment, the SiPM temperature was controlled as 27.6 ± 0.4 °C.

The total energy of an event was measured as

$$E = E_1 + E_2 . \tag{3}$$

The coincidence time was estimated by two methods, which are

$$t = \min(t_1, t_2, \ldots, t_8) - \min(t_9, t_{10}, \ldots, t_{16}), \tag{4}$$

and

$$t = mean(t_1, t_2, \ldots, t_8) - mean(t_9, t_{10}, \ldots, t_{16}), \tag{5}$$

where $t_1$ to $t_8$ are the timing outputs of a LYSO unit and $t_9$ to $t_{16}$ are the timing outputs of the LYSO slab. The first method used the earliest triggered signal to compute the coincidence time of an event, while the second method used the average timing outputs of all triggered signal. The DOI ratio was estimated as

$$\mathrm{DOI} = \frac{E_1}{E_1 + E_2}. \tag{6}$$

A DOI calibration curve was used to convert the DOI ratio to the interaction depth, which was obtained by a linear fit of the peak value of the DOI ratio histogram to the known depth of interaction. The DOI resolution was acquired by a gaussian fit of the depth histogram.

## 3. Results

The flood histograms of different light guide thicknesses are shown in figure 5. With the increase of light guide thickness, the flood histograms became uniform and the LYSO crystals in the corner were gradually more resolvable. For the 2.0 mm light guide, however, it was too thick and neighboring crystals near the sides were hard to distinguish. The concentrations of LYSO crystals in the center were brighter than those of LYSO crystals in the corner, which indicated that the LYSO crystals in the center had high detection efficiency. Based on the flood histogram, we chose light guide thickness as 1.2 mm.

The peak amplitude in ADI and energy resolution measured at different depths, energy resolution, and flood histogram of all LYSO crystals are shown in figure 6. It can be seen that the fluctuation at different depths was within one standard deviation. The average energy resolution FWHM over 10 depths was 15.66% ± 0.66% respectively, where the error is one standard deviation.

The time peak and time resolution based on two methods is shown in figure 7. The average time resolution FWHM over 10 depths were 602.98 × 10.58 ps and 763.76 ± 10.03 ps for the earliest triggered method and the mean triggered method, respectively. Using the data measured at all 10 depths, however, the timing resolution of the entire detector was 761.5 ps based on earliest triggered method and was 813 ps based on mean triggered method. The earliest triggered method achieved a better time resolution because the earliest triggered signal was the closest to the physical time when the interaction happened, thus it was more accurate. Figure 7 also shows that the standard deviation of the earliest triggered method was larger in the two ends than in the middle. The reason was that different SiPM channels had different trigger time delays. When the interaction depth was close to one end of LYSO, the SiPMs attached to this end were more likely to be triggered earlier than the SiPMs attached to the other end. As a result, the coincidence time was more variable in the ends, which resulted in the larger standard deviation.

The DOI ratio histogram of one LYSO unit and the DOI resolution FWHM measured at different depths is shown in figure 8. The average DOI resolution over 10 depths was 2.33 ± 0.07 mm.

## 4. Discussion

Figure 5 shows the tradeoff in choosing the optimal light guide. A thin light guide can resolve LYSO crystals more clearly, but the detection efficiency of LYSO crystals in the corner is low. This is because only events that trigger all 4 SiPMs on either end of the LYSO unit are selected. For a thin light guide, since the light sharing of scintillation lights from one LYSO crystal is not sufficient, it is difficult for an LYSO crystal in the corner to trigger all 4 SiPMs. For a thick light guide, though the LYSO crystals in the corner can be detected easily, the excessive light sharing makes the concentration of one LYSO crystal expanded and thus neighboring crystals are difficult to distinguish. The 1.2 mm light guide is optimal because it can resolve all LYSO crystals clearly and it has a relatively uniform detection efficiency. The flood histograms also show distortion, which is caused by the nonlinearity between the LYSO positions and the scintillation lights received by different SiPMs. A thin light guide shows a severe distortion because the spread of scintillation lights is not sufficient and most scintillation lights are received by one SiPM.

Table 1 summarizes the design and performance of some dual-ended readout detectors for high-resolution PET applications. For achieving high sensitivity, all the designs use 20 mm or longer LYSO and lutetium oxyorthosilicate (LSO). A high packing fraction is also important. Generally, the smaller LYSO crystal size is, the more reflective layers and protective layers will be needed. In our design, the packing fraction of the LYSO block is 86.5%.

The comparison also shows that our design can achieve relatively good energy, time and DOI resolution. Two reasons contribute to the balanced performance. The first reason is the accurate measurement capability of time and amplitude signals by utilizing TOFPET2 ASIC. The second reason is the careful choice of surface roughness of LYSO crystals and reflective material. A high DOI resolution prefers rough surface with a diffuse reflector

because the high likelihood of scintillation light being absorbed by or escaping from the rough surface causes a strong dependency of light collection on depth. However, the low and variable light output due to the light loss leads to a poor energy resolution. Moreover, the irregular diffuse reflection results in variations on the photon arrival time, which degrades the time resolution (Shao *et al* 2002, Bircher and Shao 2012, Ren *et al* 2014, Fan *et al* 2016). Thus, we ground the four lateral surfaces of LYSO crystals to W14, whose roughness is between the polished surface and saw-cut surface. The reflector Toray E60 is also an intermediate material between the specular reflector and diffuse reflector. We further polished the two end surfaces of LYSO crystals to improve the light collection efficiency.

## 5. Conclusion

In conclusion, a dual-ended readout detector based on SiPM and TOFPET2 ASIC is evaluated. The LYSO crystal size was $1 \times 1 \times 20$ $mm^3$, and the packing fraction of the LYSO block was 86.5%. To achieved a balanced performance, the four lateral surfaces of LYSO crystals were ground to W14, and the reflector was chosen as Toray E60. With a 1.2 mm light guide, all the crystals within an LYSO unit could be resolved. The energy, coincidence time, and DOI resolution of the detector were characterized as 15.66% ± 0.66%, 602.98 ± 10.58 ps and 2.33 ± 0.07 mm FWHM, respectively. Compared with other dual-ended detectors for high-resolution PET, our result shows superior DOI resolution. The good DOI resolution indicates the potential of utilizing the detector for high-resolution PET applications. Our next step is to design a flexible circuit to put all the readout electronics on the one end of the LYSO block to get a compact geometry and scale up the detector for image study.

## Acknowledgments

The authors would also like to thank the Cancer Scholars for Translational and Applied Research Program (C*STAR) jointly funded by Carle Foundation Hospital and the University of Illinois. We also acknowledge support from the National Institute of Biomedical Imaging and Bioengineering of the National Institutes of Health under Award Number R01EB028091.

## References

Berg E, Roncali E, Kapusta M, Du J and Cherry SR 2016 A combined time-of-flight and depth-of-interaction detector for total-body positron emission tomography Med. Phys 43 939–50 [PubMed: 26843254]

Bircher C and Shao Y 2012 Investigation of crystal surface finish and geometry on single LYSO scintillator detector performance for depth-of-interaction measurement with silicon photomultipliers Nucl. Instrum. Methods Phys. Res. A 693 236–43 [PubMed: 23087497]

Bisogni MG and Morrocchi M 2016 Development of analog solid-state photo-detectors for positron emission tomography Nucl. Instrum. Methods Phys. Res. A 809 140–8

Bugalho R et al. 2018 Experimental results with TOFPET2 ASIC for time-of-flight applications Nucl. Instrum. Methods Phys. Res. A 912 195–8

Burr KC, Ivan A, Castleberry DE, LeBlanc JW, Shah KS and Farrell R 2004 Evaluation of a prototype small-animal PET detector with depth-of-interaction encoding IEEE Trans. Nucl. Sci 51 1791–8

Di Francesco A, Bugalho R, Oliveira L, Pacher L, Rivetti A, Rolo M, Silva J, Silva R and Varela J 2016 TOFPET2: a high-performance ASIC for time and amplitude measurements of SiPM signals in time-of-flight applications J. Instrum 11 C03042

Dokhale P, Silverman R, Shah KS, Grazioso R, Farrell R, Glodo J, McClish M, Entine G, Tran V and Cherry SR 2004 Performance measurements of a depth-encoding pet detector module based on position-sensitive avalanche photodiode read-out Phys. Med. Biol 49 4293 [PubMed: 15509066]

Du J, Bai X and Cherry SR 2018 A depth-of-interaction encoding PET detector module with dual-ended readout using large-area silicon photomultiplier arrays Phys. Med. Biol 63 245019 [PubMed: 30523925]

Fan P, Ma T, Wei Q, Yao R, Liu Y and Wang S 2016 Choice of crystal surface finishing for a dual-ended readout depth-of-interaction (DOI) detector Phys. Med. Biol 61 1041 [PubMed: 26757857]

Godinez F, Chaudhari AJ, Yang Y, Farrell R and Badawi RD 2012 Characterization of a high-resolution hybrid DOI detector for a dedicated breast PET/CT scanner Phys. Med. Biol 57 3435 [PubMed: 22581109]

Ito M, Lee JS, Park MJ, Sim KS and Hong SJ 2010 Design and simulation of a novel method for determining depth-of-interaction in a PET scintillation crystal array using a single-ended readout by a multi-anode PMT Phys. Med. Biol 55 3827 [PubMed: 20551503]

Kimble T, Chou M and Chai BH 2002 Scintillation properties of LYSO crystals IEEE Nuclear Science Symp. Conf. Record vol 3 (IEEE)

Kolb A, Parl C, Mantlik F, Liu C, Lorenz E, Renker D and Pichler B 2014 Development of a novel depth of interaction PET detector using highly multiplexed G-APD cross-strip encoding Med. Phys 41 081916 [PubMed: 25086547]

Kuang Z et al. 2018 Development of depth encoding small animal PET detectors using dual-ended readout of pixelated scintillator arrays with SiPMs Med. Phys 45 613–21 [PubMed: 29222959]

Kuang Z. et al. 2019; Dual-ended readout small animal PET detector by using 0.5 mm pixelated LYSO crystal arrays and SiPMs. Nucl. Instrum. Methods Phys. Res. A. 917

Kuang Z. et al. 2017; Performance of a high-resolution depth encoding PET detector using barium sulfate reflector. Phys. Med. Biol. 62:5945. [PubMed: 28682792]

Moses W and Derenzo SE 1994 Design studies for a PET detector module using a PIN photodiode to measure depth of interaction IEEE Trans. Nucl. Sci 41 1441–5

Pizzichemi M, Stringhini G, Niknejad T, Liu Z, Lecoq P, Tavernier S, Varela J, Paganoni M and Auffray E 2016 A new method for depth of interaction determination in PET detectors Phys. Med. Biol 61 4679 [PubMed: 27245174]

Ren S, Yang Y and Cherry SR 2014 Effects of reflector and crystal surface on the performance of a depth-encoding PET detector with dual-ended readout Med. Phys 41 072503 [PubMed: 24989406]

Schaart DR, van Dam HT, Seifert S, Vinke R, Dendooven P, Löhner H and Beekman FJ 2009 A novel, SiPM-array-based, monolithic scintillator detector for PET Phys. Med. Biol 54 3501 [PubMed: 19443953]

Shao Y, Meadors K, Silverman R, Farrell R, Cirignano L, Grazioso R, Shah K and Cherry S 2002 Dual APD array readout of LSO crystals: optimization of crystal surface treatment IEEE Trans. Nucl. Sci 49 649–54

Shao Y, Sun X, Lan KA, Bircher C, Lou K and Deng Z 2014 Development of a prototype PET scanner with depth-of-interaction measurement using solid-state photomultiplier arrays and parallel readout electronics Phys. Med. Biol 59 1223 [PubMed: 24556629]

Song TY, Wu H, Komarov S, Siegel SB and Tai YC 2010 A sub-millimeter resolution PET detector module using a multi-pixel photon counter array Phys. Med. Biol 55 2573 [PubMed: 20393236]

St James S, Yang Y, Wu Y, Farrell R, Dokhale P, Shah KS and Cherry SR 2009 Experimental characterization and system simulations of depth of interaction PET detectors using 0.5 mm and 0.7 mm LSO arrays Phys. Med. Biol 54 4605 [PubMed: 19567945]

Stickel JR and Cherry SR 2004 High-resolution PET detector design: modelling components of intrinsic spatial resolution Phys. Med. Biol 50 179

Yamamoto S, Watabe H, Watabe T, Ikeda H, Kanai Y, Ogata Y, Kato K and Hatazawa J 2016 Development of ultrahigh resolution Si-PM-based PET system using 0.32 mm pixel scintillators Nucl. Instrum. Methods Phys. Res. A 836 7–12

Yamaya T, Hagiwara N, Obi T, Tsuda T, Kitamura K, Hasegawa T, Haneishi H, Inadama N, Yoshida E and Murayama H 2006 Preliminary resolution performance of the prototype system for a 4-layer DOI-PET scanner: jPET-D4 IEEE Trans. Nucl. Sci 53 1123–8

Yang Y et al. 2016 A prototype high-resolution small-animal PET scanner dedicated to mouse brain imaging J. Nucl. Med 57 1130–5 [PubMed: 27013696]

Yang Y, Wu Y, Qi J, James SS, Du H, Dokhale PA, Shah KS, Farrell R and Cherry SR 2008 A prototype PET scanner with DOI-encoding detectors J. Nucl. Med 49 1132–40 [PubMed: 18552140]

Yeom JY, Vinke R and Levin CS 2014 Side readout of long scintillation crystal elements with digital SiPM for TOF-DOI PET Med. Phys 41 122501 [PubMed: 25471979]

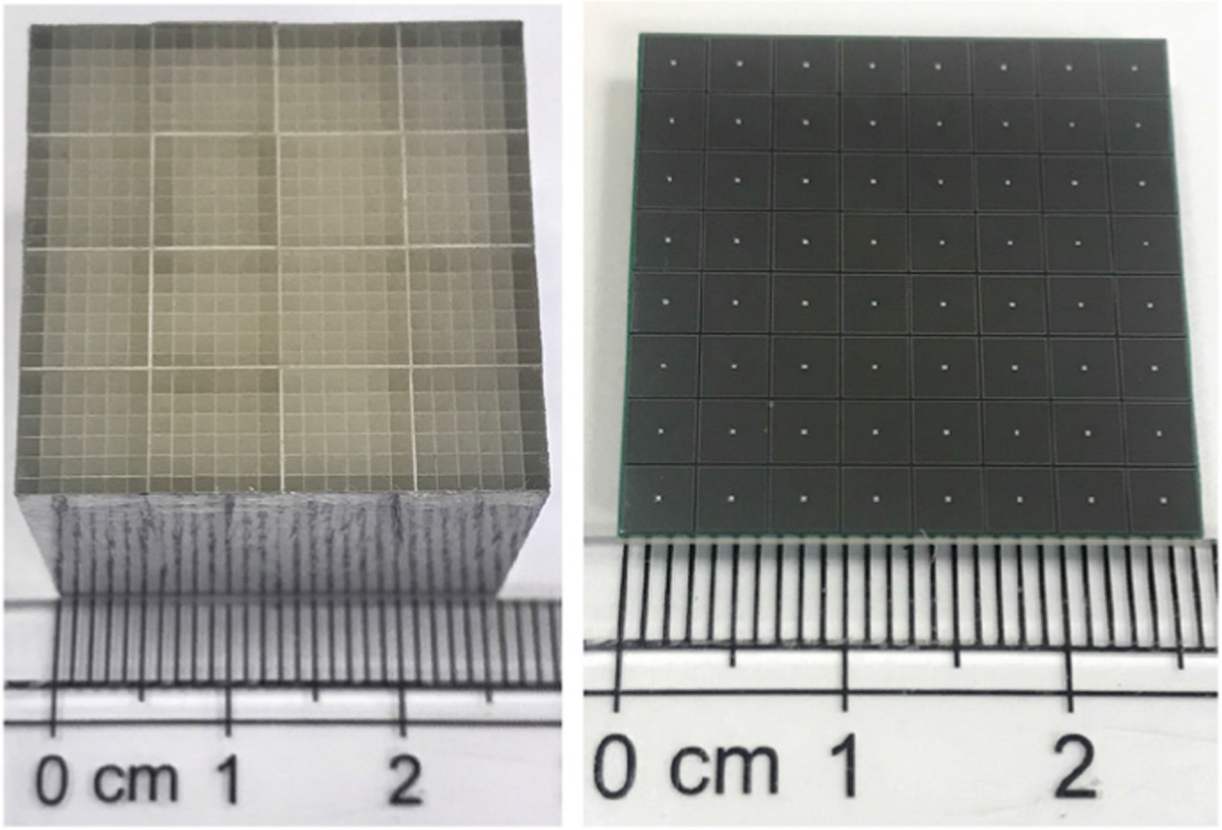


**Figure 1.**

Left: the LYSO block contains 4 × 4 LYSO unit. Right: the Hamamatsu A13361 3050AE-08 SiPM array contains 8 × 8 SiPM channels. Both the LYSO block and the SiPM array are 25.8 × 25.8 $mm^2$. A LYSO unit is read out by two 2 × 2 SiPM arrays.

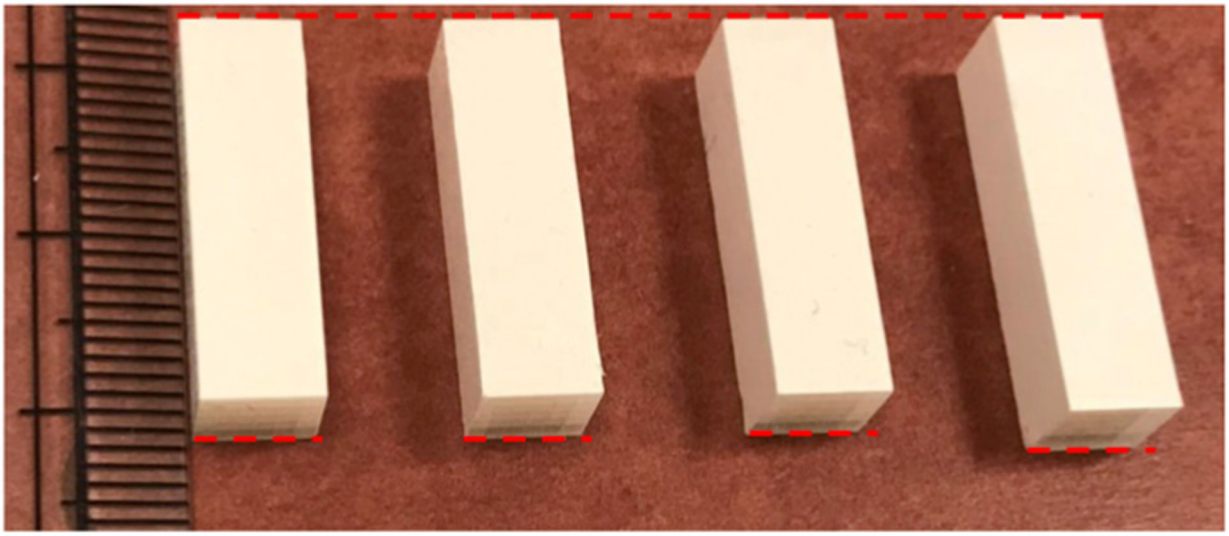

**Figure 2.**
Four LYSO units with different light guide thicknesses (from left to right are 0.8, 1.0, 1.2, and 2.0 mm) were fabricated.

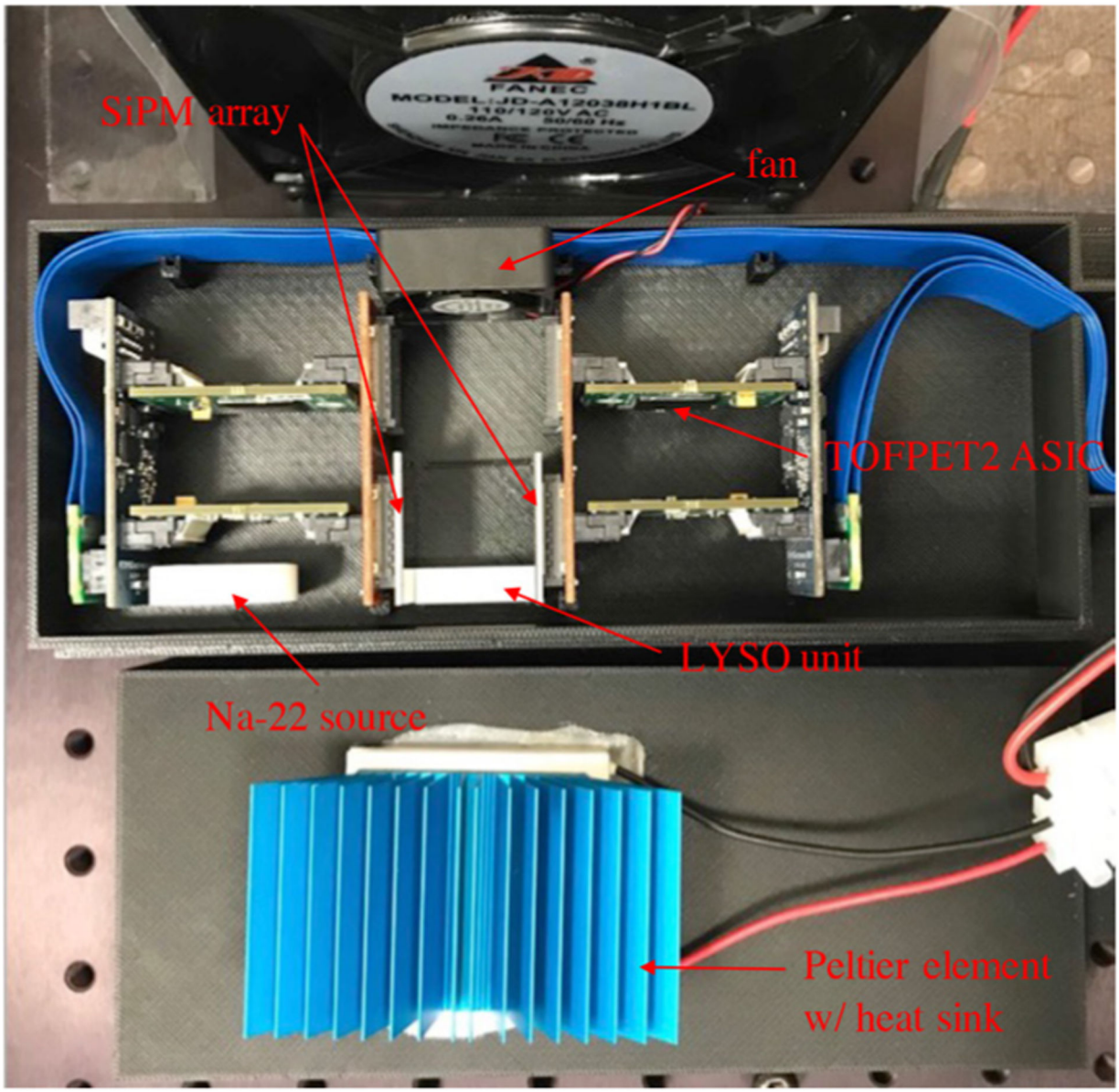


**Figure 3.**
The experiment setup for measuring the optimal light guide thickness.

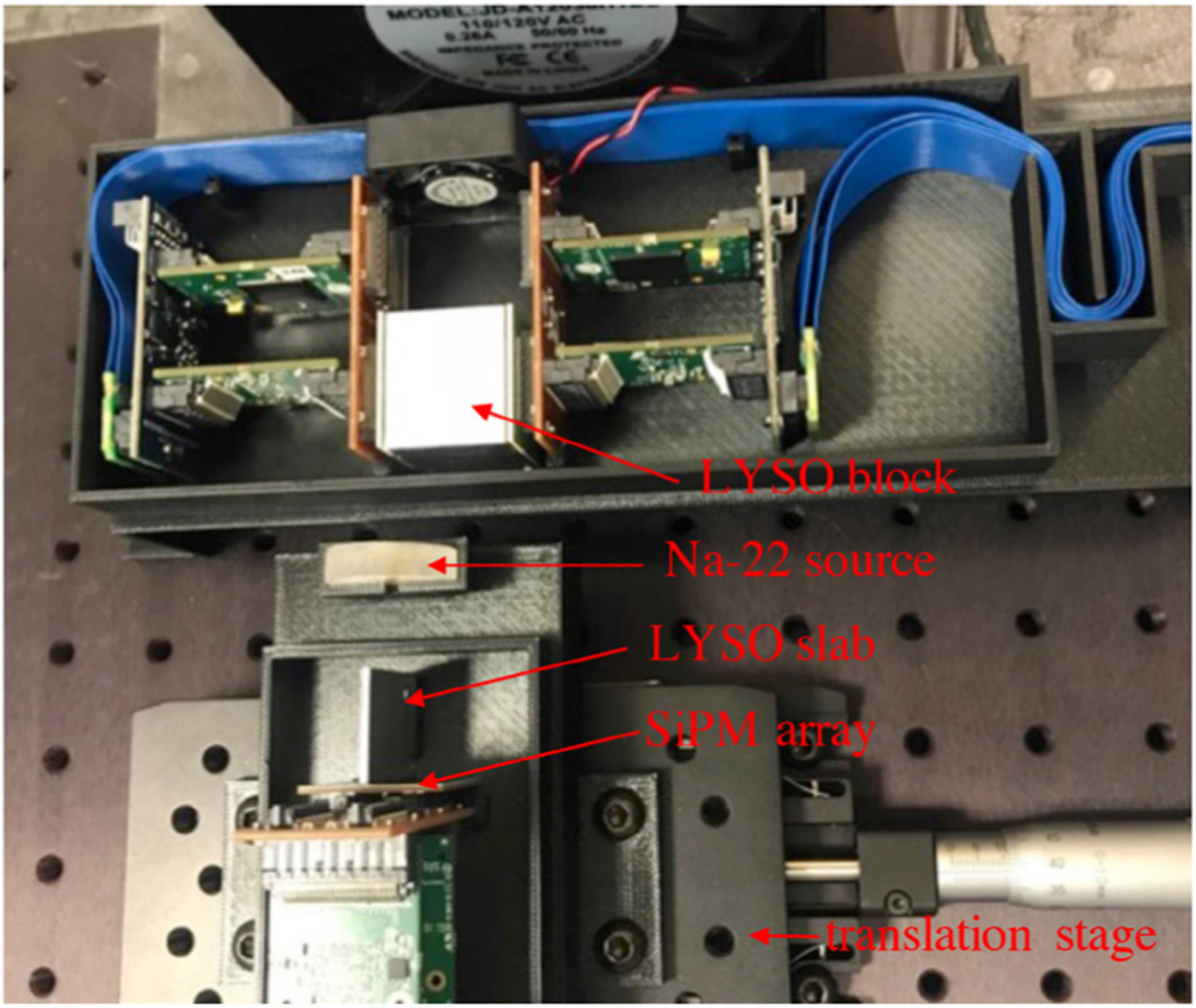


**Figure 4.**
The experiment setup for measuring the energy, time and DOI resolution at different depths.

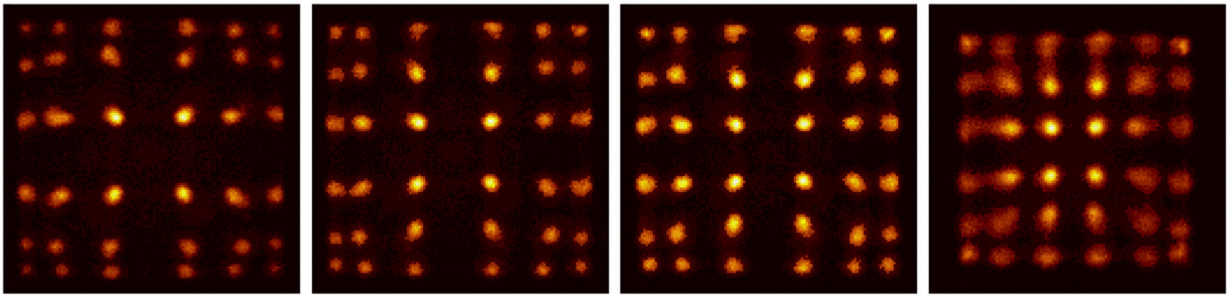

**Figure 5.**
The flood histograms of different light guide thicknesses. For left to right: 0.8, 1.0, 1.2 and 2.0 mm.

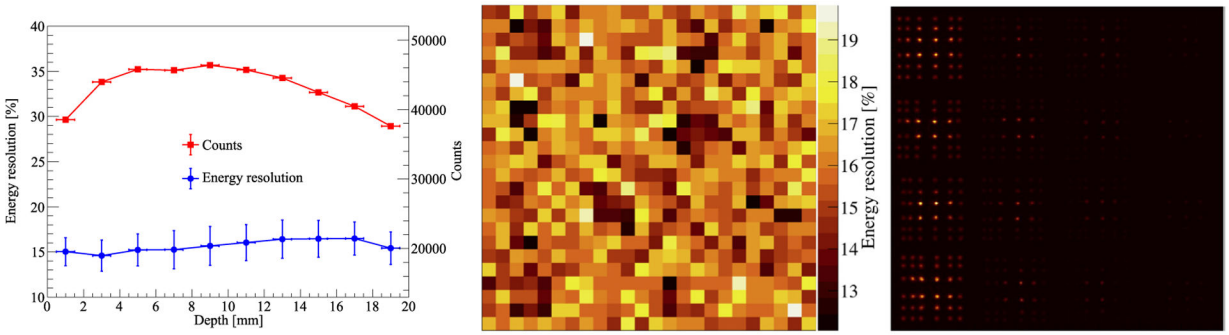


**Figure 6.**

Left: Energy peak amplitude in ADI and energy resolution at 10 depths. The vertical error bar is the standard deviation over 16 LYSO units. The horizontal error bar is the 1 mm interaction depth error. Middle: The energy resolution of all LYSO crystals computed over all depths. Right: The flood histogram of all LYSO crystals over all depths.

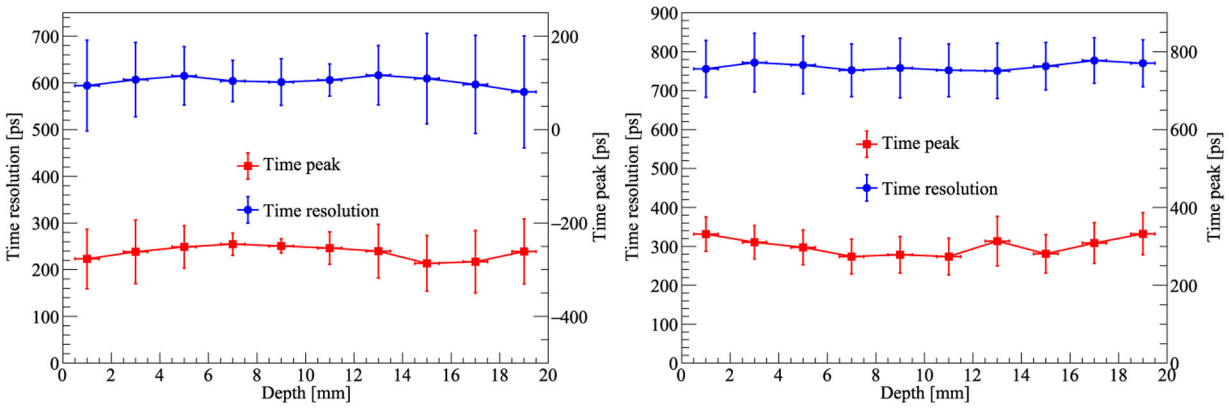


**Figure 7.**

Left: time peak and time resolution at 10 depths based on the earliest triggered method equation (4). Right: time peak and time resolution at 10 depths based on mean triggered method equation (5).

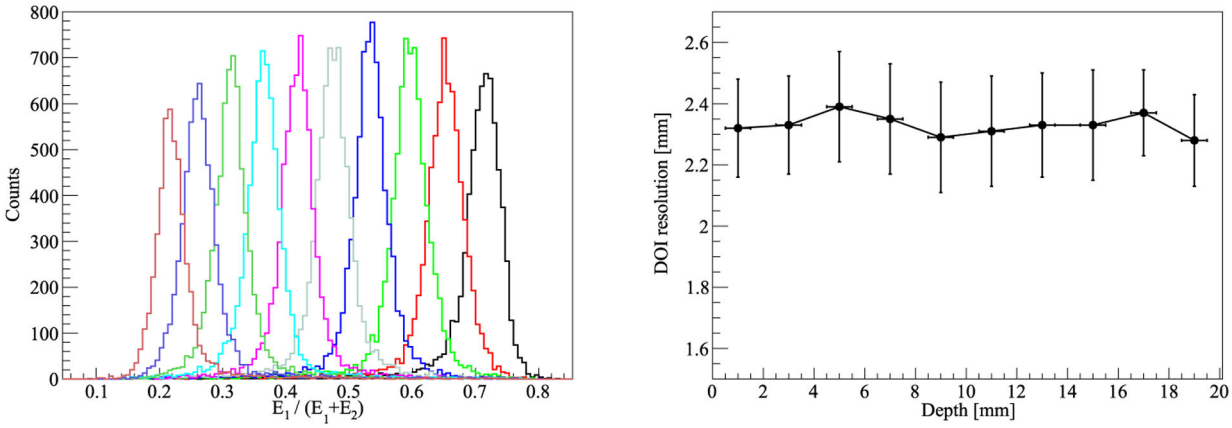


**Figure 8.**

Left: DOI profile of one LYSO unit at 10 depths. The depth distance between neighboring peaks is 2 mm. Right: DOI resolution at 10 depths.

**Table 1.**

Design and performance of high-resolution dual-ended readout PET detectors.

| Citation | Crystal ($mm^3$) | Detector | Energy (%) | Time (ns) | DOI (mm) |
|---|---|---|---|---|---|
| — | LYSO 1 × 1 × 20 | SiPM | 15.66 | 0.60 | 2.33 |
| Godinez *et al* (2012) | LYSO 1.5 × 1.5 × 20 | PSPMT[a] + APD | 19 | 2.4 | 2.9 |
| Kolb *et al* (2014) | LSO 1.55 × 1.55 × 20 | G-APD[a] | 12.8 | 1.14 | 2.9 |
| Shao *et al* (2014) | LYSO 1.9 × 1.9 × 30 | SSPM[a] | 17.6 | 2.8 | 5.6 |
| Kuang *et al* (2018) | LYSO 0.97 × 0.97 × 20 | SiPM | 16.7 | 1.41 | 2.1 |
| Du *et al* (2018) | LYSO 0.95 × 0.95 × 20 | SiPM | 23.8 | 1.78 | 2.81 |
| Kuang *et al* (2019) | LYSO 0.5 × 0.5 × 20 | SiPM | 21 | 1.23 | 2.84 |

[a]PSPMT: position-sensitive photomultiplier tube. G-APD: Geiger mode avalanche photodiode. SSPM: solid-state photomultiplier.